Analytica Chimica Acta, Volume 1283, December 2023, Article Number 341947
DOI: 10.1016/j.aca.2023.341947

Poly-Adenine-Mediated Tetrahedral DNA Nanostructure with Multiple Target-Recognition Sites for Ultrasensitive and Rapid Electrochemical Detection of Aflatoxin B1

Kaixuan Wang[1], Nuanfei Zhu[1], Yumo Li[1], Hu Zhang[1], Beibei Wu[2], Jian Cui[3], Jun Tang[2], Zhugen Yang[4], Fang Zhu[1], Zhen Zhang[1*]*

[1] School of Emergency Management, School of the Environment and Safety Engineering, Jiangsu University, Zhenjiang 212013, China.

[2] Zhejiang Provincial Center for Disease Control and Prevention, Hangzhou 310015, China.

[3] Institute of Botany, Jiangsu Province and Chinese Academy of Sciences (Nanjing Botanical Garden Mem. Sun Yat-Sen), Nanjing 210014, China.

[4] School of Water, Energy, and Environment, Cranfield University, Milton Keynes MK43 0AL, U.K.

*Corresponding author:

E-mail: jtang@cdc.zj.cn, zhangzhen@ujs.edu.cn

Fax: +86-511-88790955

ABSTRACT

Tetrahedral DNA nanostructures (TDNs) are widely used in the development of

Published by Elsevier. This is the Author Accepted Manuscript issued with: Creative Commons Attribution Non-Commercial No Derivatives License (CC:BY:NC:ND 4.0).
The final published version (version of record) is available online at DOI:10.1016/j.aca.2023.341947. Please refer to any applicable publisher terms of use.

electrochemical biosensors due to their structural stability, programmability, and strong interfacial orderliness. However, the complex modifications on the electrode and the single vertex target recognition of the TDNs limit their applications in electrochemical biosensing. Herein, we developed a universal detection system based on a novel polyadenine-based tetrahedral DNA nanostructure (ATDN) using Aflatoxin B1 (AFB1) as the model target for analysis. In the absence of target AFB1, the signal probes (SP) modified with ferrocene would be anchored by five aptamers on ATDN. The target capture by aptamers led to a release of SP from the electrode surface, resulting in a significant reduction of the electrochemical signal. This new nanostructure was not only dispensed with multi-step electrode modifications and strong mechanical rigidity but also had five modification sites which enhanced the detection sensitivity for the target. As a result, this biosensor shows good analytical performance in the linear range of 1 fg mL^{-1} to 1 ng mL^{-1}, exhibiting a low detection limit of 0.33 fg mL^{-1}. Satisfactory accuracy has also been demonstrated through good recoveries (95.2%-98.9%). The proposed new tetrahedral DNA nanostructure can provide a more rapid and sensitive alternative to previous electrochemical sensors based on the conventional TDN. Since DNA sequences can be designed flexibly, the sensing platform in this strategy can be extended to detect various targets in different fields.

Keywords: Signal amplification; Aflatoxin B1; Electrochemical biosensor; Rapid detection; Aptamer.

1. Introduction

Benefiting from their high sensitivity, easy programmability, and fast response [1-3],

electrochemical biosensors are considered a promising tool in many fields including disease diagnosis [4-7], food safety [8-10], and environmental monitoring [11-13]. Among these sensors, aptamer-based electrochemical biosensors have shown obvious advantages and attracted so much attention. Aptamers, a kind of nucleic acids or peptide molecules, have a specific affinity binding to target molecules which are similar to antibody-antigen pairs and can be synthesized using standard methods [14-17]. Compared with other recognition molecules, the application of aptamers overcame some limitations such as low specificity, poor stability, complex synthesis, and high degradability [18, 19]. However, single strands of aptamers are usually nonrigid structures, and some problems such as uneven density and entanglement often occur during the process of immobilization on the electrode surface [20]. These obvious deficiencies usually inhibit the binding activity between the aptamer and targets, in turn affecting the sensitivity and stability of biosensors [19, 21]. Therefore, it is crucial to design a novel strategy that can improve the capture efficiency between the aptamer and target to construct highly stable aptamer-based electrochemical biosensors.

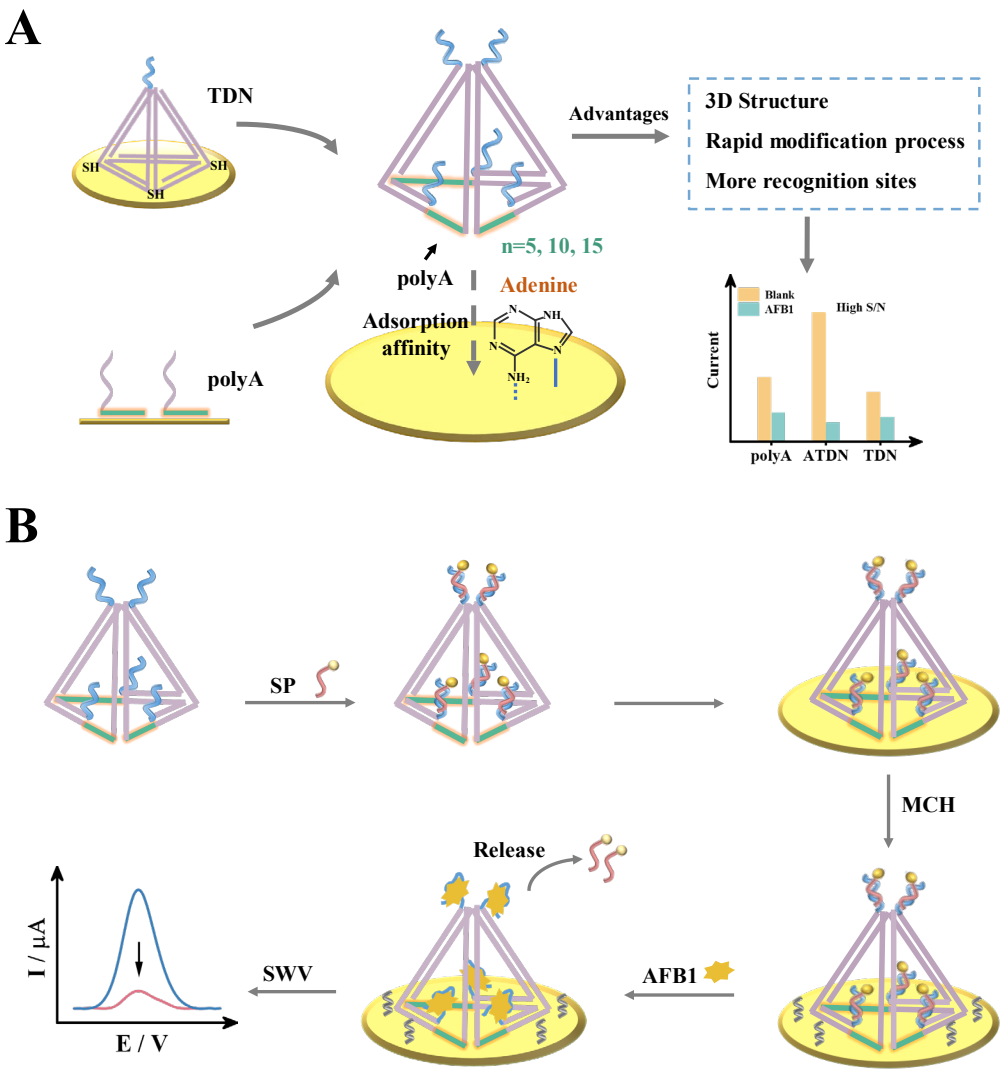
In recent years, tetrahedral DNA nanostructures (TDNs), which possess high 3D mechanical rigidities and good programmability [19, 22-25], have attracted intense interest in the application of electrochemical biosensors [26-31]. In particular, the TDNs have unparalleled advantages of regulating the distance between the probes on the electrode [32] and possession of more electrode surface sites [20, 21], increasing the accessibility of the probe-target interactions, then further improving the detection sensitivity. In addition, according to their excellent programmability, TDNs have been

proposed as scaffolds for the construction of multifunctional nanoprobes to achieve functionalization with different chemical and biological molecules[33-35]. However, three vertices of TDNs are completely occupied by thiol modification, resulting in fewer available binding sites for the probe on the tetrahedron surface. And the overnight thiol modification makes the immobilization on the electrode quite time-consuming. These factors have led to a limited performance in electrochemical biosensing. To solve these problems, the polyadenine (polyA) composed of consecutive adenine nucleotides has been applied to assemble probes on the gold surface. Different from conventional thiol-DNA probes, the unlabeled polyA can be immobilized on the gold electrode by the covalent binding of adenine to the gold surface as an effective anchor block [2, 8, 36]. Hence, it is urgent to design a DNA nanostructure that can be rapidly and stably modified on an electrode with good interface regulation ability, as a highly sensitive and versatile sensing platform.

Herein, we designed a novel polyadenine-based tetrahedral DNA nanostructure (ATDN) for the development of electrochemical aptasensors. The preparation processes of the ATDN and biosensor are illustrated in **Scheme 1**. First, four well-designed DNA single strands were utilized to construct the ATDN which involved three polyA segments on the bottom and Aflatoxin B1 (AFB1) aptamers at five vertices. Signal probes (SP) with ferrocene at the 5-terminal could be anchored by aptamers along, resulting in a notable electrochemical signal. When the AFB1 was introduced, the aptamers would capture the target specifically and release the SP from the electrode surface, inducing the decreased electrochemical signal dramatically. This strategy

89 greatly improves detection efficiency when it combines the advantages of polyA probes
90 and conventional tetrahedral DNA nanostructure: great density and orientation control
91 ability, stable anchoring without any group modification process, and multi-vertex
92 recognition ability. Based on optimized conditions, this electrochemical DNA biosensor
93 demonstrates successful detection of AFB1 in real samples with remarkable sensitivity.

Scheme 1. Schematic Diagrams of the developed Novel Tetrahedral DNA Nanostructure (Part A) and the Principle of the Biosensing Platform for Sensitive AFB1 Detection (Part B).



2. Experiment section

2.1. Materials and Reagents

The signal probe was purchased from Sangon Biotechnology Company, Ltd. (Shanghai, China). Other DNA oligonucleotides were synthesized and purified by Nanjing GenScript Biotechnology Co., Ltd. (Nanjing, China). The sequences are listed in **Table S1**. The 6-Mercaptohexanol (MCH) was purchased from Meryer Chemical

Technology Company, Ltd. Hybridization buffer (Tris-HCl buffer, pH 7.4) comprised 20 mM, Tris, 140 mM NaCl, and 50 mM $MgCl_2$. $[Fe(CN)_6]^{3-/4-}$ solution contained 5 mM $K_4[Fe(CN)_6]$, 5 mM $K_3[Fe(CN)_6]$, and 0.1 M KCl. All other reagents are of analytical grade. Ultrapure water was used for cleaning the electrodes and preparing aqueous solutions (Milli-Q, 18 MΩ·cm^{-1} resistivity at 25 °C, Merck Millipore).

2.2. Self-Assembly of the tetrahedral DNA probe

The ATDN were prepared as previous reports: The four single strands (L_A, L_B, L_C, and L_D) were first dissolved in TE buffer to a concentration of 100 μM, then diluted to 1 μM with Tris-HCl buffer for further processing [37, 38]. To form ATDN, equal molar amounts of four DNA strands were heated at 95°C for 10 min. Then the product was rapidly cooled to 4°C and kept for 30 min. Finally, the SP was mixed with ATDN at a 5:1 molar ratio for 120 min at 37°C to form ATDN/SP. The DNA sequences are listed in **Table S1**.

2.3. Construction of the electrochemical biosensor

The fabrication process of the proposed electrochemical biosensor is shown in Scheme 1. Firstly, gold electrodes with a diameter of 2 mm were cleaned [39]. Then, 1 μM 3 μL of prepared ATDN/SP solution was added dropwise on the treated gold electrode. After the reaction at 37°C for 2 h, the ATDN/SP was anchored to the gold electrode by the covalent binding between the bottom adenine and the surface. Finally, the MCH (3 μL, 0.5 mM) was dropped onto the electrode surface for 10 min incubation at 4°C to block the non-specific binding sites.

2.4. Electrochemical measurements

Cyclic voltammetry (CV), electrochemical impedance spectroscopy (EIS), and square wave voltammetry (SWV) measurements were performed on a CHI Model 660E electrochemical workstation (CH Instruments, inc.). Throughout the experiment, a three-electrode system consisting of an Au working electrode, an Ag/AgCl reference electrode, and a platinum counter electrode was utilized. Both CV and EIS electrochemical measurements were tested in $[Fe(CN)_6]^{3-/4-}$ solution. The CV measurement was carried out at a scan rate of 100 mV/s over a potential range of -0.2 to 0.6 V. The EIS was recorded by a frequency range from 10^{-1} to 10^5 Hz with an amplitude of 5 mV. The SWV measurement was performed in PBS solution (including different concentrations of AFB1) at a potential ranging from -0.5 to 0.1 V. And other parameters are as follows: potential increment of 4 mV, amplitude width of 25 mV, and frequency of 50 Hz. To ensure accuracy, each measurement was repeated a minimum of three times.

3. Results And Discussion

3.1. Characterization of ATDN

The agarose gel electrophoresis (AGE) was conducted to verify the assembly process of ATDN. Firstly, the step-by-step assembly of ATDN is shown in **Fig. 1A and B**. It can be seen that the migration speed of the electrophoretic bands decreased accordingly after the gradual assembly of DNA strands. And lane 4 showed the slowest migration, indicating the successful formation of ATDN. Then, **Fig. 1C** illustrated the successful operation of the proposed biosensor in the presence of the target. In detail, lane 1 to lane 4 corresponded to SP, ATDN, ATND/SP, and ATDN/SP/AFB1 separately. When

AFB1 was mixed with ATND/SP, two separate bands appeared, which represented the band of lane 1 and a new band with slower mobility. This phenomenon demonstrated the success of the target-ATDN binding and the release of the signal probe. Next, atomic force microscopy (AFM) was employed to confirm the characterization of ATDN. As observed in **Fig. 1D**, there are lots of evenly distributed bright dots with the typical morphology of DNA tetrahedrons in the AFM image. The force-distance curves of ATDN demonstrated that the height also corresponded to the relevant height of DNA tetrahedrons[30, 40]. Moreover, the dynamic light scattering (DLS) and zeta potential were used to further verify the sizes of ATDN and ATDN/SP. According to the result of DLS in **Fig. 1F**, the ATDN was found to have a hydrodynamic diameter of approximately 6.24 nm, which was close to the theoretical edge length of 6.12 nm [40]. By comparison, the average size increased gradually after the addition of SP and AFB1, indicating the formation of ATDN/SP and the process of aptamer-target capture. The zeta potential changed from 5.85 mV to 7.85 mV with the assembly of SP (**Fig. 1G**), further demonstrating the successful construction process of ATDN/SP and ATDN/SP/AFB1. The above results showed that ATDN and ATDN/SP were well prepared by our preplanned design.

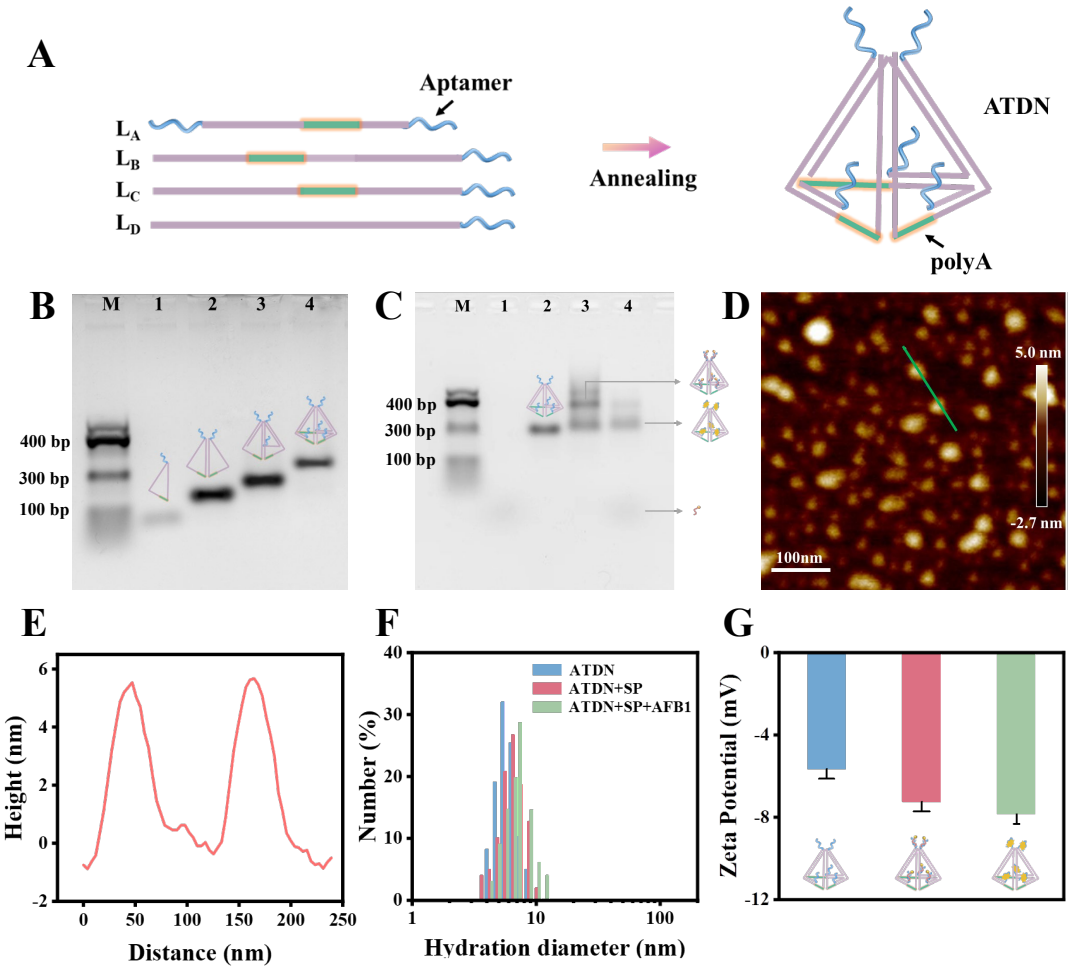


Fig. 1. (A) Diagrammatic sketch of synthesis of ATDN. AGE characterization of (B) step-by-step preparation of ATDN and (C) operation of the proposed biosensor in the presence of target AFB1. (D) AFM image and (E) force-distance curves of ATDN. (F) DLS of ATDN and ATDN/SP. (G) Zeta potential analysis of ATDN and ATDN/SP.

3.2. Electrochemical Characterization of the Electrode

To evaluate the stepwise modification of the electrode, cyclic voltammetry (CV) and electrochemical impedance spectroscopy (EIS) were performed. The well-defined CV redox peak was observed at the bare Au electrode (**Fig. 2A**, curve a). When the assembled ATDN/SP was modified on the electrode, a significant decrease in the redox peak was observed, which was attributed to the low conductivity of the DNA

tetrahedron (curve b). Subsequently, owing to the introduction of MCH, the electron transfer was impeded, causing the redox peak to decrease correspondingly (curve c). Finally, the redox peak (curve d) was further decreased after AFB1 was added.

Meanwhile, EIS was also used to expound and prove the stepwise modification process in **Fig. 2B**. Usually, the bare Au electrode had an extremely narrow semicircle (as shown by curve a) due to its high conductivity. Since the low conductivity of the DNA tetrahedron could enhance the electron transfer resistance, the semicircle increased after the introduction of ATDN/SP (curve b). When treating the surface of the Au electrode with MCH, the R_{et} of the Au electrode enhanced again because of the blocked electron transport path (curve c). Finally, after AFB1 was captured by ATDN, the semicircle (curve d) further increased as expected, revealing the successful fabrication of the biosensor. Both the CV and EIS results confirmed that the electrochemical biosensing platform was successfully constructed.

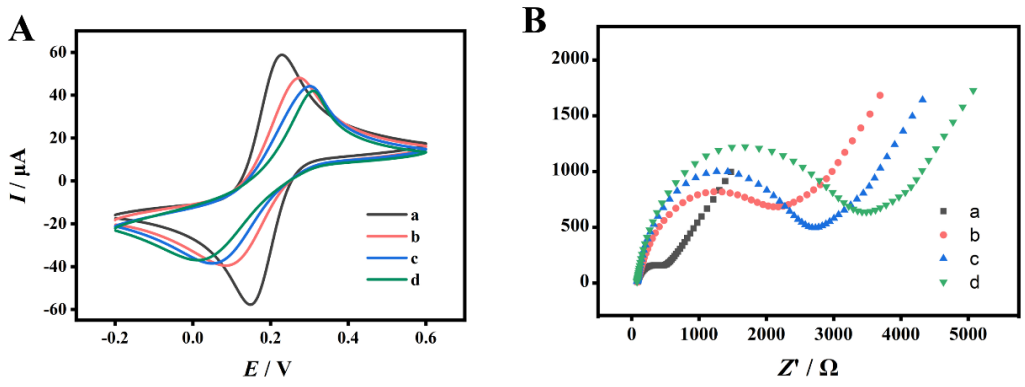


Fig. 2. (A) CV and (B) EIS response of (a) bare Au electrode, (b) ATDN+SP /Au, (c) MCH/ ATDN+SP /Au, (d) AFB1/ MCH/ ATDN+SP /Au.

3.3.Feasibility of the Proposed Biosensor

SWV measurements were performed to certify the feasibility of the biosensor (with

30 nt polyA-based-ATDN) for AFB1 detection. As depicted in **Fig.3**, in the absence of AFB1, a significant SWV signal could be observed. By comparison, in the presence of 10 pg mL^{-1} AFB1, the signal decreased significantly, showing that the biosensor could be validly used to detect the target AFB1.

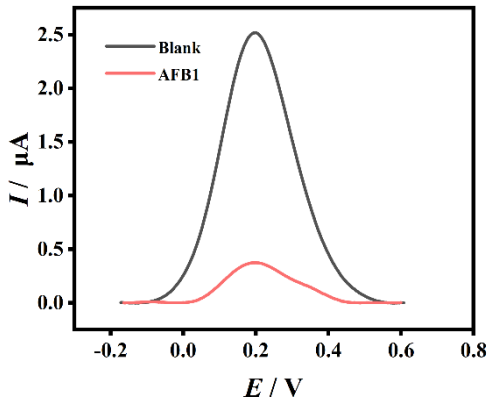


Fig. 3. SWV results of the proposed biosensor with and without 10 pg mL^{-1} AFB1.

3.4. Study of the ATDN Assembling

As the length of polyA at the bottom was closely related to the fixing efficiency of ATDN on the gold electrode, the PolyA sequences with different total lengths (15, 30, 45 nt) were compared and analyzed in the presence of 10 pg mL^{-1} AFB1 (**Fig. 4A**). The AGE, CV, EIS, and SWV results were illustrated in **Fig. S1 and S2** respectively. Initially, the assembly conditions of those ATDNs were authenticated by AGE. As seen in **Fig. S1A**, ATDN with 15 nt polyA was synthesized successfully. When the length of the ATDN increased to 45 nt polyA, the preparation of ATDN failed (**Fig. S2A**). The main reason for this phenomenon was that the long polyA length hindered the combination of the double-stranded parts at the bottom, affecting the performance of 45 nt-ATDN. Although tetrahedral synthesis was partial successful according to AGE results, the resulted tetrahedral could also be modified on the gold electrode together

with 30 nt of polyA. Subsequently, SWV and signal/noise ratio were utilized to further verify the electrochemical performance of ATDN. As shown in **Fig. 4B**, when the total length of the polyA fragment increased from 15 nt to 30 nt, there was a gradual decrease in the current signal, accompanied by an increase in the blank signal. This phenomenon may be attributed to the weak fixation performance of the 15 nt polyA on the gold electrode. The highest S/ N (6.8) was achieved when the polyA sequence was 30 nt. As the length of polyA reached 45 nt, a noticeable decrease in the current signal was observed, probably because the undesirable ATDN construction reduced the capture efficiency of the aptamer and target. Therefore, ATDN with the polyA length of 30 nt was employed for AFB1 detection owing to the highest target capture efficiency.

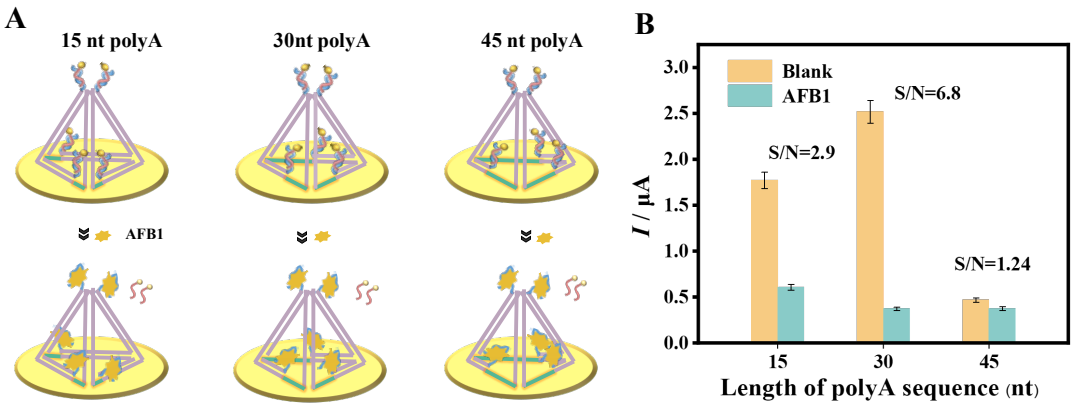


Fig. 4. (A) Schematic illustration of 15nt polyA-based ATDN as type a, 30nt polyA-based ATDN as type b, 45nt polyA-based ATDN as type c. (B) SWV peak currents of three types ATDN in the (a) absence and (b) presence of the target AFB1 (10 pg mL^{-1}).

3.5.Signal enhancement using the ATDN

To verify the signal enhancement of our ATDN biosensor, we designed the other two different capture probes including polyA (30 nt) and conventional TDN for comparison under the identical recognition aptamer sequence and conditions (**Fig. 5A**). The CV,

EIS, and SWV curves with good results were observed (**Fig. S3 and S4**). By assembly with the same concentration (1 μM) using three types of DNA probes, the target response signal of 10 pg mL^{-1} AFB1 was measured. Then, the detection sensitivities of the three probes were compared by employing the signal/noise ratio (S/N). As noted, the biosensor based on the ATDN probe achieved higher S/N (6.8) than those of polyA and TDN probes (**Fig. 5B**). The reason was that the ATDN was modified with more aptamers and the ATDN-based biosensor could generate stronger electrochemical signals according to the design. To explore the reasons more clearly, ATDN was also designed to modify two aptamers and compared with polyA at the same concentration (1 μM) and conditions (**Fig. S5**). According to **Fig. S5B**, without the influence of the different aptamer numbers, ATDN showed better detection sensitivity and higher S/N ratio, indicating better interface controllability of ATDN on the electrode compared to polyA. Its advantage of multi-modification was also performed through the comparison between1 μM ATDN and TDN in **Fig. 5B**. Then, three probes at the same aptamer concentration were compared to further test the performance, and the total product of the probe number and the probe concentration were required to be consistent the same (5 μM). As shown in **Fig. 5A**, the number of aptamers designed on the three probes was different (two aptamers on the polyA, five aptamers on the ATDN, and one aptamer on the TDN). Therefore, the concentration of polyA and TDN were calculated as 2.5 μM and 5 μM, respectively, and then compared at the same conditions. As depicted in **Fig. 5C**, the S/N of ATDN was still the highest while the background signal of polyA and TDN increased significantly, which was the result of a better capture efficiency due to

its lower surface density of ATDN on the electrode. Moreover, the lowest background signal of ATDN is consistent with the result of S/N. These results indicated the ATDN-based biosensor showed better performance of signal response and sensitivity.

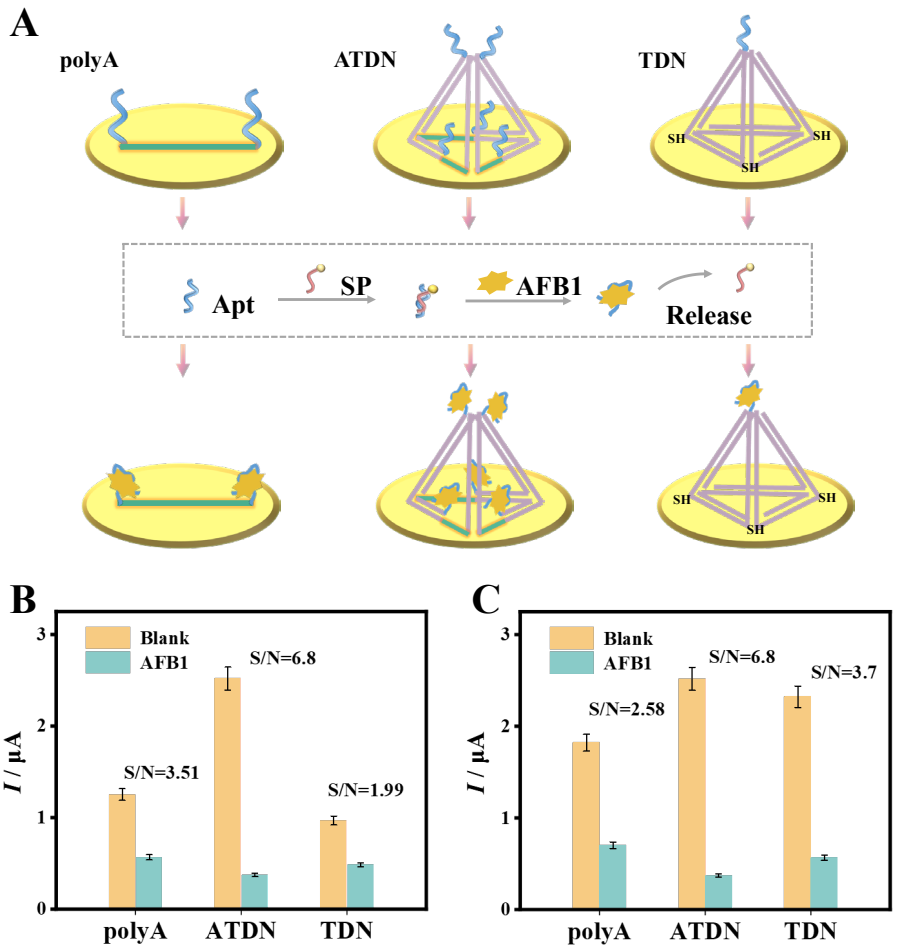


Fig. 5. Signal enhancement in electrochemical AFB1 analysis. (A) Schematic of AFB1 detection with three different DNA capture probes (polyA, ATDN, and TDN). (B) SWV peak currents of three 1 μM DNA capture probes in the (a) absence and (b) presence of the target AFB1 (10 pg mL^{-1}). (C) SWV peak currents of three DNA capture probes with different concentrations (2.5 μM polyA, 1 μM ATDN, and 5 μM TDN) in the (a) absence and (b) presence of the target AFB1 (10 pg mL^{-1}).

3.6. Optimization of the Experimental Conditions.

To explore the best electrochemical analysis performance of the biosensor, some important parameters were optimized. The distribution density of ATDN on the electrode was studied by controlling the ATDN concentration on the electrode when the AFB1 was 10 pg mL^{-1}. **Fig. S6A** manifested the change in current response caused by ATDN ranging from 0.6 μM to 1.4 μM. It can be seen that the peak current went up with the increase in ATDN concentrations. After the maximum value of 1.0 μM, the current decreased due to the high surface density on the electrode. Hence, 1.0 μM was the optimum concentration of ATDN on the Au electrode in this work. Furthermore, the modification of the signal label was also important for the electrochemical performance of the biosensor, thus the reaction time of ATDN and SP was optimized. As depicted in **Fig. S6B**, the electrochemical signal increased over time and attained the maximum after 120 min, then declined rapidly. Therefore, 120 min was chosen as the optimum reaction time. Finally, the detection time of the target AFB1 was also optimized in **Fig. S6C**. The current approached a stable value after a reaction time of 40 min, implying that 40 min was the optimal reaction time.

3.7. Performance of the Electrochemical Biosensor

To evaluate the analytical performance, different concentrations of AFB1 were measured by performing SWV under optimal experimental conditions. The peak SWV current was correlated with the concentration of signal probes on the ATDN. Thus, the performance of the electrochemical biosensor could be analyzed by the intensity of the peak SWV current. As depicted in **Fig. 6A**, the SWV signal tended to decrease with AFB1 concentration increasing, which was consistent with our proposed strategy. The

resulting plots showed that there was a good linear correlation between the logarithm of the AFB1 concentration ranging from 1 fg mL^{-1} to 1 ng mL^{-1} and the SWV response, following a linear regression equation of I=-1.088+0.45 log c with a correlation coefficient of 0.9894 (**Fig. 6B**). And the detection limit of this biosensor was 0.33 fg mL^{-1} (S/N = 3). In comparison to the previously reported methods for AFB1 detection in **Table 1**, this electrochemical biosensor exhibits excellent and rapid analytical performance.

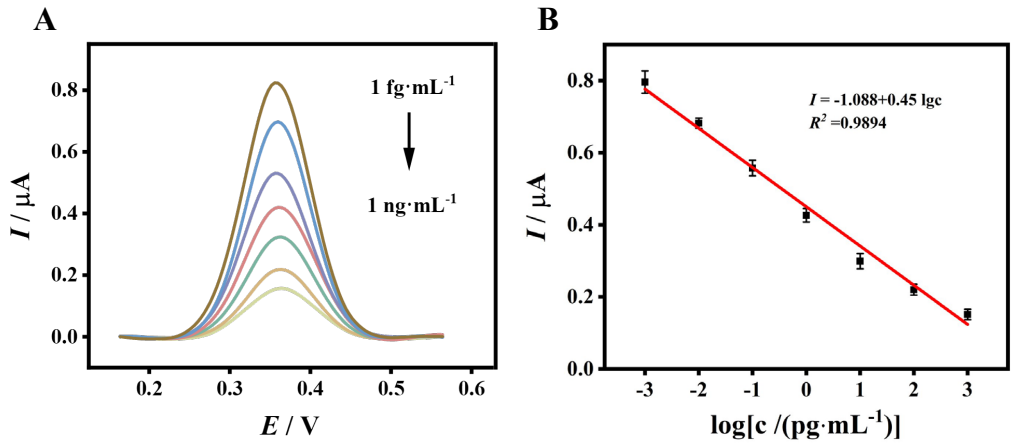


Fig. 6. (A) SWV responses of the biosensor towards different concentrations of AFB1: 0.001 pg mL^{-1}, 0.01 pg mL^{-1}, 0.1 pg mL^{-1}, 1 pg mL^{-1}, 10 pg mL^{-1}, 100 pg mL^{-1}, and 1000 pg mL^{-1}. (B) Calibration curve of SWV peak current value versus the logarithm of AFB1 concentration.

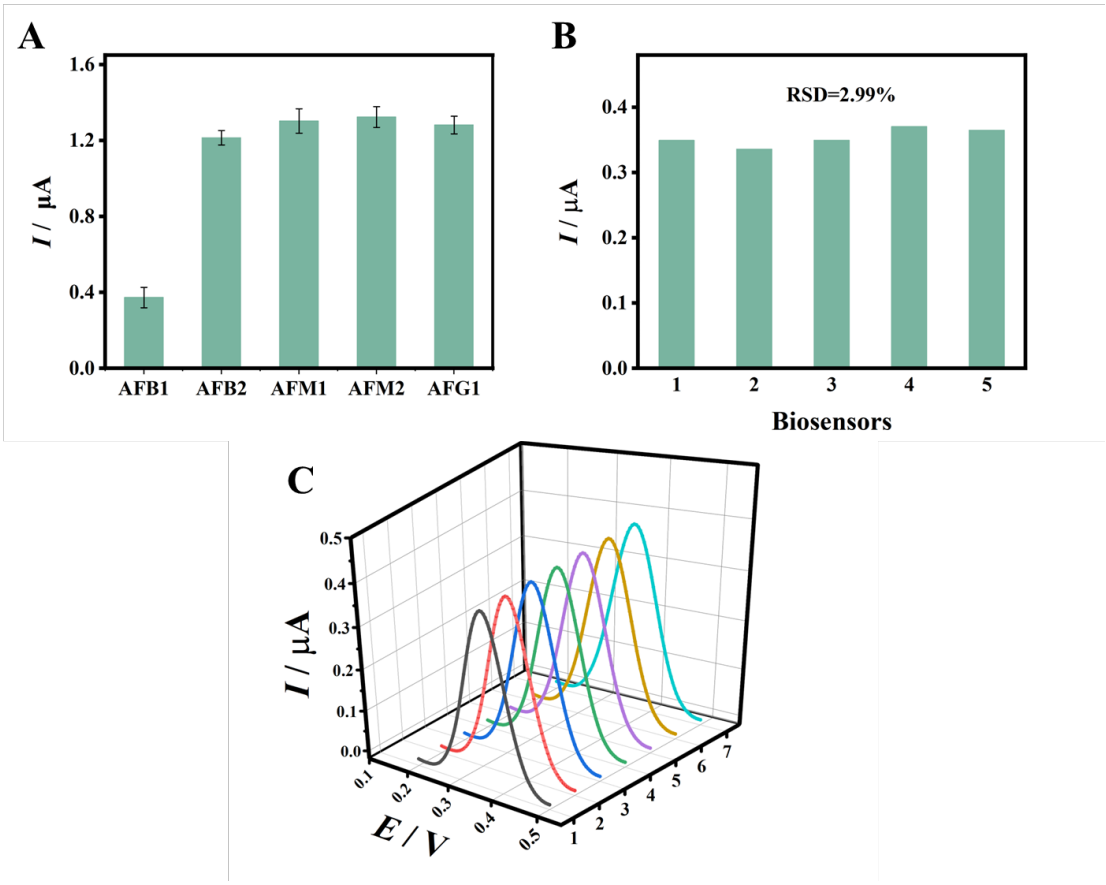
Table 1

Analytical performances of various reported methods for AFB1 detection.

Detection method	Consuming time (h)	Linear range	Detection limit	Refs
Fluorescence	>24	1 to 1000 pg mL^{-1}	0.492 pg mL^{-1}	[41]
Fluorescence	>24	0 to 20 ng mL^{-1}	0.27 ng mL^{-1}	[42]
Fluorescence	>24	0.001 to 80 ng mL^{-1}	0.92 pg mL^{-1}	[43]
pMRS	>24	10 pg mL^{-1} to 10 ng mL^{-1}	0.35 pg mL^{-1}	[44]
SERS	>24	0.01 pg mL^{-1} to 1 ng mL^{-1}	5.07 fg mL^{-1}	[45]
ECL	22	1.0 fg mL^{-1} to 10 ng mL^{-1}	0.58 fg mL^{-1}	[46]
ECL	>24	1.0 pg mL^{-1} to 100 ng mL^{-1}	4.56 fg mL^{-1}	[47]
SWV	14	2 nM to 4 μM	2 nM	[48]
LSV	>24	0.05 to 100 ng mL^{-1}	0.43 pg mL^{-1}	[49]
DPV	>24	0.1 pg mL^{-1} to 1 μg mL^{-1}	4.81 fg mL^{-1}	[50]
DPV	>24	0.1 to 1000 pg mL^{-1}	0.03 pg mL^{-1}	[51]
ACV	>24	0.01 to 3.0 ng mL^{-1}	4.3 pg mL^{-1}	[52]
SWV	**5.4**	**1.0 fg mL^{-1} to 1 ng mL^{-1}**	**0.33 fg mL^{-1}**	**This work**

3.8. Selectivity, stability, and reproducibility of the biosensor

Selectivity, stability, and reproducibility were performed to comprehensively assess the performance of the biosensor proposed in this work. To evaluate the selectivity of the biosensing platform, the AFB1 analogs including AFB2, AFM1, AFM2, and AFG1, were tested under the same conditions (**Fig. 7A**). It was found that only the AFB1 could cause a significant decrease in the signal response, while the current response of other aflatoxins was negligible. The results indicated that this prepared biosensor had good selectivity for AFB1. Furthermore, as seen in **Fig. 7B**, the relative standard deviation (RSD) was 2.99% (n=5), demonstrating acceptable reproducibility. For stability, the as-prepared biosensor was stored at 4 ℃ and the SWV value retained 96.8% of its initial current value after 7 days (**Fig. 7C**), manifesting good stability of this biosensor.



316

317 **Fig. 7.** (A) Specificity of the biosensor in AFB1, AFB2, AFM1, AFM2, and AFG1 (10

318 pg mL^{-1} AFB1). (B) Reproducibility (10 pg mL^{-1} AFB1) of the biosensor. (C) Stability

319 of the prepared biosensor (7 days with 10 pg mL^{-1} AFB1).

320 *3.9. Analysis of AFB1 in real samples*

321 To verify the applicability of this biosensor, we analyzed corn samples spiked with

322 0.5, 1, 5, and 10 ng mL^{-1} AFB1 for recovery experiments. Referring to a previous study

323 [53], artificially fortified corn samples were extracted. The specific experimental steps

324 were shown in supporting information. The resulting samples were re-diluted using

325 PBS and then utilized for AFB1 detection, as shown in **Table S2**. Under the same

326 conditions, all samples were tested, and the recoveries of AFB1 ranged from

327 95.2%－98.9%. These results indicate that our proposed aptamer sensor has good

applicability in real samples. Also, the detection results were used to compare with the HPLC method [19]. Satisfactory results indicate that our established biosensor has good accuracy and applicability for the detection of AFB1 in real samples.

4. Conclusion

In summary, we have designed a novel DNA tetrahedron incorporating polyA (ATDN) and multi-target recognition for the rapid and sensitive electrochemical detection of AFB1. In this strategy, the ATDN not only binds rapidly to gold electrodes without modification of the thiol but also has the strong spatial modulation capability of the TDN. Besides, the ATDN had more linkage sites than the TDN, further improving the detection sensitivity. Through comprehensive parameter optimizations and assessments, the proposed biosensor showed remarkable selectivity, satisfactory sensitivity (LOD= 0.33 fg mL^{-1}) with a wide working range between 1 fg mL^{-1} to 1 ng mL^{-1}, and acceptable recoveries (95.2%−98.9%). Overall, this described approach provided a new idea for establishing a rapid, efficient and sensitive biosensing platform. We also believe that this novel sensing platform can be applied to the detection of various targets.

Acknowledgements

This work was supported by the National Natural Science Foundation of China (Grants No. 22176075 and 21876067), the special scientific research project of School of Emergency Management, Jiangsu University (KY-C-02, KY-D-06), the Student Scientific Research Project from Jiangsu University (Grant No. 22A105) and the Jiangsu Collaborative Innovation Center of Technology and Material of Water Treatment.

References

[1] S. Su, J. Ma, Y. Xu, H. Pan, D. Zhu, J. Chao, L. Weng, L. Wang, Electrochemical Analysis of Target-Induced Hairpin-Mediated Aptamer Sensors, ACS Appl Mater Interfaces, 12 (2020) 48133-48139.

[2] Y. Wang, D. Xiong, J. Wang, J. Cheng, J. Xiao, S. Yakubu, K. Wang, J. Lv, Z. Zhang, Triblock polyadenine probe-based electrochemical DNA sensor by integrating 3D DNAzyme walker and strand displacement for ultrasensitive and rapid detection of Pb2+, Sensors and Actuators B: Chemical, 347 (2021).

[3] J. Wu, W. Lv, Q. Yang, H. Li, F. Li, Label-free homogeneous electrochemical detection of MicroRNA based on target-induced anti-shielding against the catalytic activity of two-dimension nanozyme, Biosens Bioelectron, 171 (2021) 112707.

[4] Z. Ge, M. Lin, P. Wang, H. Pei, J. Yan, J. Shi, Q. Huang, D. He, C. Fan, X. Zuo, Hybridization chain reaction amplification of microRNA detection with a tetrahedral DNA nanostructure-based electrochemical biosensor, Anal Chem, 86 (2014) 2124-2130.

[5] Z. Zhang, P. Sen, B.R. Adhikari, Y. Li, L. Soleymani, Development of Nucleic-Acid-Based Electrochemical Biosensors for Clinical Applications, Angew Chem Int Ed Engl, 61 (2022) e202212496.

[6] Y. Tang, Y. Dai, X. Huang, L. Li, B. Han, Y. Cao, J. Zhao, Self-Assembling Peptide-Based Multifunctional Nanofibers for Electrochemical Identification of Breast Cancer Stem-like Cells, Anal Chem, 91 (2019) 7531-7537.

[7] X. Liu, X. Gao, L. Yang, Y. Zhao, F. Li, Metal-Organic Framework-Functionalized Paper-Based Electrochemical Biosensor for Ultrasensitive Exosome Assay, Anal Chem,

93 (2021) 11792-11799.

[8] L. Wang, Y. Wen, X. Yang, L. Xu, W. Liang, Y. Zhu, L. Wang, Y. Li, Y. Li, M. Ding, S. Ren, Z. Yang, M. Lv, J. Zhang, K. Ma, G. Liu, Ultrasensitive Electrochemical DNA Biosensor Based on a Label-Free Assembling Strategy Using a Triblock polyA DNA Probe, Anal Chem, 91 (2019) 16002-16009.

[9] T. Chaibun, O.V.C. La, A.P. O'Mullane, B. Lertanantawong, W. Surareungchai, Fingerprinting Green Curry: An Electrochemical Approach to Food Quality Control, ACS Sens, 3 (2018) 1149-1155.

[10] Y. Zhang, Y. Lei, H. Lu, L. Shi, P. Wang, Z. Ali, J. Li, Electrochemical detection of bisphenols in food: A review, Food Chem, 346 (2021) 128895.

[11] Y. Li, Y. Chang, J. Ma, Z. Wu, R. Yuan, Y. Chai, Programming a Target-Initiated Bifunctional DNAzyme Nanodevice for Sensitive Ratiometric Electrochemical Biosensing, Analytical Chemistry, 91 (2019) 6127-6133.

[12] K. Mao, H. Zhang, Z. Wang, H. Cao, K. Zhang, X. Li, Z. Yang, Nanomaterial-based aptamer sensors for arsenic detection, Biosensors and Bioelectronics, 148 (2020).

[13] W. Kang, X. Pei, C.A. Rusinek, A. Bange, E.N. Haynes, W.R. Heineman, I. Papautsky, Determination of Lead with a Copper-Based Electrochemical Sensor, Anal Chem, 89 (2017) 3345-3352.

[14] X. Zhang, R.A. Lazenby, Y. Wu, R.J. White, Electrochromic, Closed-Bipolar Electrodes Employing Aptamer-Based Recognition for Direct Colorimetric Sensing Visualization, Anal Chem, 91 (2019) 11467-11473.

[15] Y. Xiao, B.D. Piorek, K.W. Plaxco, A.J. Heeger, A Reagentless Signal-On

Architecture for Electronic, Aptamer-Based Sensors via Target-Induced Strand Displacement, Journal of the American Chemical Society, 127 (2005) 17990-17991.

[16] F. Kleinjung, S. Klussmann, V.A. Erdmann, F.W. Scheller, J.P. Fürste, F.F. Bier, High-Affinity RNA as a Recognition Element in a Biosensor, Analytical Chemistry, 70 (1998) 328-331.

[17] J. Liu, S. Wagan, M. Dávila Morris, J. Taylor, R.J. White, Achieving Reproducible Performance of Electrochemical, Folding Aptamer-Based Sensors on Microelectrodes: Challenges and Prospects, Analytical Chemistry, 86 (2014) 11417-11424.

[18] Y. Liu, L. Kong, H. Li, R. Yuan, Y. Chai, Electrochemical Aptamer Biosensor Based on ATP-Induced 2D DNA Structure Switching for Rapid and Ultrasensitive Detection of ATP, Anal Chem, 94 (2022) 6819-6826.

[19] G. Peng, X. Li, F. Cui, Q. Qiu, X. Chen, H. Huang, Aflatoxin B1 Electrochemical Aptasensor Based on Tetrahedral DNA Nanostructures Functionalized Three Dimensionally Ordered Macroporous MoS(2)-AuNPs Film, ACS Appl Mater Interfaces, 10 (2018) 17551-17559.

[20] L. Yu, L. Zhu, M. Yan, S. Feng, J. Huang, X. Yang, Electrochemiluminescence Biosensor Based on Entropy-Driven Amplification and a Tetrahedral DNA Nanostructure for miRNA-133a Detection, Anal Chem, 93 (2021) 11809-11815.

[21] H. Pei, N. Lu, Y. Wen, S. Song, Y. Liu, H. Yan, C. Fan, A DNA nanostructure-based biomolecular probe carrier platform for electrochemical biosensing, Adv Mater, 22 (2010) 4754-4758.

[22] N. Lu, H. Pei, Z. Ge, C.R. Simmons, H. Yan, C. Fan, Charge transport within a

three-dimensional DNA nanostructure framework, J Am Chem Soc, 134 (2012) 13148-13151.

[23] Q.M. Feng, Z. Zhou, M.X. Li, W. Zhao, J.J. Xu, H.Y. Chen, DNA tetrahedral scaffolds-based platform for the construction of electrochemiluminescence biosensor, Biosens Bioelectron, 90 (2017) 251-257.

[24] S. Ma, Y. Zhang, Q. Ren, X. Wang, J. Zhu, F. Yin, Z. Li, M. Zhang, Tetrahedral DNA nanostructure based biosensor for high-performance detection of circulating tumor DNA using all-carbon nanotube transistor, Biosens Bioelectron, 197 (2022) 113785.

[25] X. Gao, X. Li, X. Sun, J. Zhang, Y. Zhao, X. Liu, F. Li, DNA Tetrahedra-Cross-linked Hydrogel Functionalized Paper for Onsite Analysis of DNA Methyltransferase Activity Using a Personal Glucose Meter, Anal Chem, 92 (2020) 4592-4599.

[26] C. Mao, W. Pan, X. Shao, W. Ma, Y. Zhang, Y. Zhan, Y. Gao, Y. Lin, The Clearance Effect of Tetrahedral DNA Nanostructures on Senescent Human Dermal Fibroblasts, ACS Appl Mater Interfaces, 11 (2019) 1942-1950.

[27] Q. Zhang, S. Lin, S. Shi, T. Zhang, Q. Ma, T. Tian, T. Zhou, X. Cai, Y. Lin, Anti-inflammatory and Antioxidative Effects of Tetrahedral DNA Nanostructures via the Modulation of Macrophage Responses, ACS Appl Mater Interfaces, 10 (2018) 3421-3430.

[28] L. He, D.Q. Lu, H. Liang, S. Xie, C. Luo, M. Hu, L. Xu, X. Zhang, W. Tan, Fluorescence Resonance Energy Transfer-Based DNA Tetrahedron Nanotweezer for Highly Reliable Detection of Tumor-Related mRNA in Living Cells, ACS Nano, 11

(2017) 4060-4066.

[29] D. Zeng, L. San, F. Qian, Z. Ge, X. Xu, B. Wang, Q. Li, G. He, X. Mi, Framework Nucleic Acid-Enabled Programming of Electrochemical Catalytic Properties of Artificial Enzymes, ACS Appl Mater Interfaces, 11 (2019) 21859-21864.

[30] J. Wang, K. Wang, H. Peng, Z. Zhang, Z. Yang, M. Song, G. Jiang, Entropy-Driven Three-Dimensional DNA Nanofireworks for Simultaneous Real-Time Imaging of Telomerase and MicroRNA in Living Cells, Anal Chem, 95 (2023) 4138-4146.

[31] L. Yang, X. Yin, B. An, F. Li, Precise Capture and Direct Quantification of Tumor Exosomes via a Highly Efficient Dual-Aptamer Recognition-Assisted Ratiometric Immobilization-Free Electrochemical Strategy, Anal Chem, 93 (2021) 1709-1716.

[32] N. Dong, D. Liu, S. Meng, S. Liu, T. You, Tetrahedral DNA nanostructure-enabled electrochemical aptasensor for ultrasensitive detection of fumonisin B1 with extended dynamic range, Sensors and Actuators B: Chemical, 354 (2022).

[33] R. Jia, X. He, W. Ma, Y. Lei, H. Cheng, H. Sun, J. Huang, K. Wang, Aptamer-Functionalized Activatable DNA Tetrahedron Nanoprobe for PIWI-Interacting RNA Imaging and Regulating in Cancer Cells, Anal Chem, 91 (2019) 15107-15113.

[34] D. Wang, Y. Chai, Y. Yuan, R. Yuan, Precise Regulation of Enzyme Cascade Catalytic Efficiency with DNA Tetrahedron as Scaffold for Ultrasensitive Electrochemical Detection of DNA, Anal Chem, 91 (2019) 3561-3566.

[35] D. Tang, W. Fan, M. Xiong, M. Li, B. Xiong, X.B. Zhang, Topological DNA Tetrahedron Encapsulated Gold Nanoparticle Enables Precise Ligand Engineering for Targeted Cell Imaging, Anal Chem, 93 (2021) 17036-17042.

[36] L. Li, L. Wang, Q. Xu, L. Xu, W. Liang, Y. Li, M. Ding, A. Aldalbahi, Z. Ge, L. Wang, J. Yan, N. Lu, J. Li, Y. Wen, G. Liu, Bacterial Analysis Using an Electrochemical DNA Biosensor with Poly-Adenine-Mediated DNA Self-Assembly, ACS Appl Mater Interfaces, 10 (2018) 6895-6903.

[37] W. Hu, Y. Chang, J. Huang, Y. Chai, R. Yuan, Tetrahedral DNA Nanostructure with Multiple Target-Recognition Domains for Ultrasensitive Electrochemical Detection of Mucin 1, Anal Chem, 94 (2022) 6860-6865.

[38] Y. Wen, H. Pei, Y. Wan, Y. Su, Q. Huang, S. Song, C. Fan, DNA nanostructure-decorated surfaces for enhanced aptamer-target binding and electrochemical cocaine sensors, Anal Chem, 83 (2011) 7418-7423.

[39] X.L. Huo, H. Yang, W. Zhao, J.J. Xu, H.Y. Chen, Nanopore-Based Electrochemiluminescence for Detection of MicroRNAs via Duplex-Specific Nuclease-Assisted Target Recycling, ACS Appl Mater Interfaces, 9 (2017) 33360-33367.

[40] X. Hui, C. Yang, D. Li, X. He, H. Huang, H. Zhou, M. Chen, C. Lee, X. Mu, Infrared Plasmonic Biosensor with Tetrahedral DNA Nanostructure as Carriers for Label-Free and Ultrasensitive Detection of miR-155, Adv Sci (Weinh), 8 (2021) e2100583.

[41] Q. Wang, F. Zhao, Q. Yang, W. Wu, Graphene oxide quantum dots based nanotree illuminates AFB1: Dual signal amplified aptasensor detection AFB1, Sensors and Actuators B: Chemical, 345 (2021).

[42] Z.H. Shao, A. Zhai, Y. Hua, H.L. Mo, F. Xie, X. Zhao, G. Zhao, S.Q. Zang,

Development of Au(8) nanocluster-based fluorescent strip immunosensor for sensitive detection of aflatoxin B(1), Anal Chim Acta, 1274 (2023) 341576.

[43] Z. Wu, D.W. Sun, H. Pu, Q. Wei, A novel fluorescence biosensor based on CRISPR/Cas12a integrated MXenes for detecting Aflatoxin B1, Talanta, 252 (2023) 123773.

[44] J. Zhao, Z. Wang, Y. Chen, D. Peng, Y. Xianyu, Horseradish peroxidase-catalyzed formation of polydopamine for ultra-sensitive magnetic relaxation sensing of aflatoxin B(1), J Hazard Mater, 419 (2021) 126403.

[45] J. Li, W. Wang, H. Zhang, Z. Lu, W. Wu, M. Shu, H. Han, Programmable DNA Tweezer-Actuated SERS Probe for the Sensitive Detection of AFB(1), Anal Chem, 92 (2020) 4900-4907.

[46] Z. Li, H. Xu, Z. Zhang, X. Miao, DNA tetrahedral scaffold-corbelled 3D DNAzyme walker for electrochemiluminescent aflatoxin B(1) detection, Food Chem, 407 (2023) 135049.

[47] X. Lv, F. Tan, T. Miao, B. Cui, J. Zhang, Y. Fang, Y. Shen, In situ generated PtNPs to enhance electrochemiluminescence of multifunctional nanoreactor COP T4VTP6 for AFB1 detection, Food Chemistry, 399 (2023).

[48] C. Wang, Y. Li, Q. Zhao, A signal-on electrochemical aptasensor for rapid detection of aflatoxin B1 based on competition with complementary DNA, Biosens Bioelectron, 144 (2019) 111641.

[49] J. Qian, C. Ren, C. Wang, K. An, H. Cui, N. Hao, K. Wang, Gold nanoparticles mediated designing of versatile aptasensor for colorimetric/electrochemical dual-

channel detection of aflatoxin B1, Biosens Bioelectron, 166 (2020) 112443.

[50] G. Wei, Q. Fan, N. Hong, H. Cui, W. Zhang, M. Rustam, A. Alim, T. Jiang, H. Dong, H. Fan, A Reagentless Aptamer Sensor Based on a Self-Powered DNA Machine for Electrochemical Detection of AFB1, Electrocatalysis, 14 (2023) 593-601.

[51] H. Cui, K. An, C. Wang, Y. Chen, S. Jia, J. Qian, N. Hao, J. Wei, K. Wang, A disposable ratiometric electrochemical aptasensor with exonuclease I-powered target recycling amplification for highly sensitive detection of aflatoxin B1, Sensors and Actuators B: Chemical, 355 (2022).

[52] C. Zhu, D. Liu, Y. Li, S. Ma, M. Wang, T. You, Hairpin DNA assisted dual-ratiometric electrochemical aptasensor with high reliability and anti-interference ability for simultaneous detection of aflatoxin B1 and ochratoxin A, Biosens Bioelectron, 174 (2021) 112654.

[53] W.B. Shim, M.J. Kim, H. Mun, M.G. Kim, An aptamer-based dipstick assay for the rapid and simple detection of aflatoxin B1, Biosens Bioelectron, 62 (2014) 288-294.

Supplementary Material

Poly-Adenine-Mediated Tetrahedral DNA Nanostructure with Multiple Target-Recognition Sites for Ultrasensitive and Rapid Electrochemical Detection of Aflatoxin B1

Kaixuan Wang[1], Nuanfei Zhu[1], Yumo Li[1], Hu Zhang[1], Beibei Wu[2], Jian Cui[3], Jun Tang[2], Zhugen Yang[4], Fang Zhu[1], Zhen Zhang[1*]*

[1] School of Emergency Management, School of the Environment and Safety Engineering, Jiangsu University, Zhenjiang 212013, China.

[2] Zhejiang Provincial Center for Disease Control and Prevention, Hangzhou 310015, China.

[3] Institute of Botany, Jiangsu Province and Chinese Academy of Sciences (Nanjing Botanical Garden Mem. Sun Yat-Sen), Nanjing 210014, China.

[4] School of Water, Energy, and Environment, Cranfield University, Milton Keynes MK43 0AL, U.K.

*Corresponding author:

E-mail: jtang@cdc.zj.cn, zhangzhen@ujs.edu.cn

Fax: +86-511-88790955

Table of Contents

Supplementary Methods

Fig. S1. Stepwise Characterization and feasibility of the 15 nt polyA-based ATDN.

Fig. S2. Stepwise Characterization and feasibility of the 45 nt polyA-based ATDN.

Fig. S3. Stepwise Characterization and feasibility of the polyA.

Fig. S4. Stepwise Characterization and feasibility of the TDN.

Fig. S5. SWV curves of polyA and ATDN with two aptamers.

Fig. S6. Optimization of experimental conditions.

Fig. S7. Detailed sequence diagram of tetrahedral DNA nanostructure.

Table S1. List of the DNA Sequences

Table S2. AFB1 detection in real samples.

Supplementary Methods

Characterization methods of ATDN structure.

The assembly process of ATDN was verified by agarose gel electrophoresis, atomic force microscope and dynamic light scanning experiments. First, 2% agarose gel was freshly prepared. DNA samples were combined with DNA loading buffer in a 5:1 volume ratio. The electrophoresis ran at 100V for 40 min in 1X TBE buffer, and all data and images were collected and analyzed by Bio-Rad imaging apparatus (Hercules, CA, USA). The AFM image was recorded with a Bruker NanoWizard 4 BioScience Atomic Force Microscope (Karlsruhe, Germany), and the experimental data was collected and analyzed using the JPK imaging process software.

Analysis of AFB1 in the real sample.

Referring to a previous study[1], artificially fortified corn samples were extracted. After grinding the corn, 1.0 g of the resulting powder was thoroughly mixed with 1 mL of methanol with the known concentrations of AFB1. Subsequently, the mixture was placed in a fume hood for 12 h, allowed to dry, and then extracted with a 2:8 volume ratio of methanol/water at room temperature for 15 min. The extract solution was filtered through a 0.45 μM filter and diluted with PBS buffer to final AFB1 concentrations (0.5, 1, 5, 10 ng mL^{-1}).

Stepwise Characterization and Feasibility of the 15nt polyA-based ATDN.

Use AGE to verify synthesis of the tetrahedral structures, and verify the stepwise assembly of electrodes using CV and EIS. The agarose electropherogram in **Figure S1A** showed that ATDN with 15 nt polyA a could be synthesized successfully, while the ATDN with 45 nt polyA in **Figure S2A** was poorly synthesized. Both CV and EIS showed that they could be successfully modified on electrodes. Finally, the SWV responses of two biosensors under different concentrations of AFB1 were recorded (**Figure S1D and S2D**).

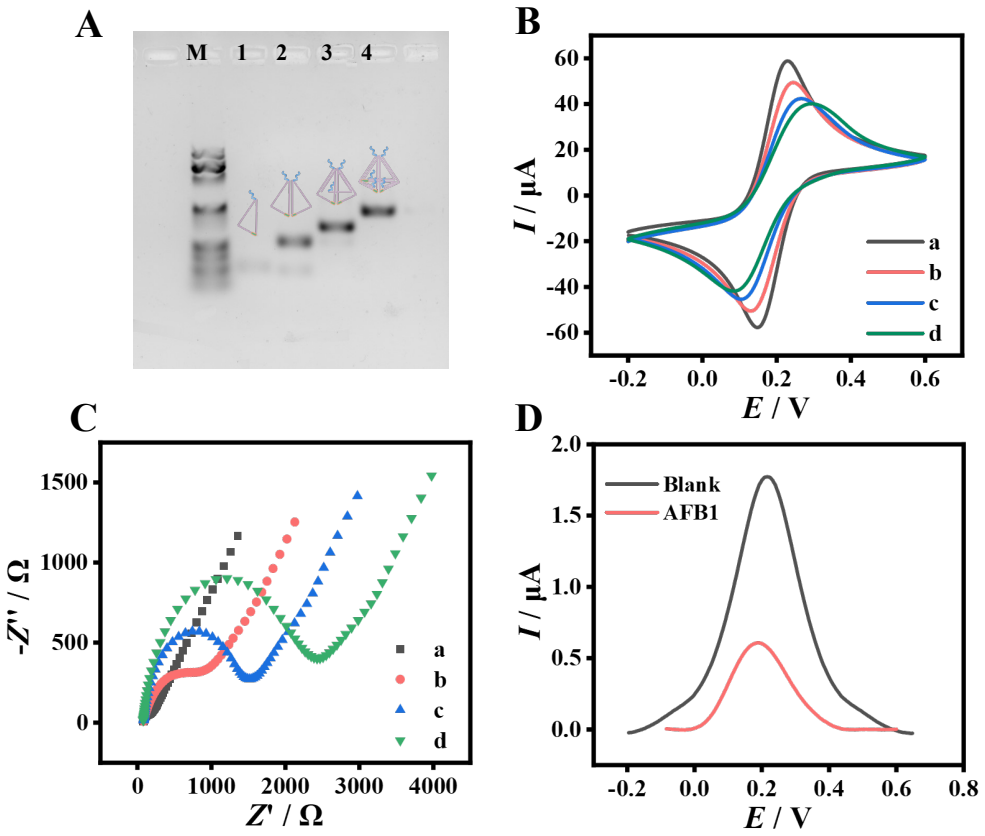


Figure S1. Characterization of 15nt-ATDN. (A) AGE. (B) CV and (C) EIS response of (a) bare Au electrode, (b) 15nt-ATDN+SP/Au, (c) MCH/15nt-ATDN+SP/Au, (d) AFB1/MCH/15nt-ATDN+SP/Au. (D) SWV in the presence and absence of 10 pg mL^{-1} AFB1.

Stepwise Characterization and Feasibility of the 45nt polyA-based ATDN.

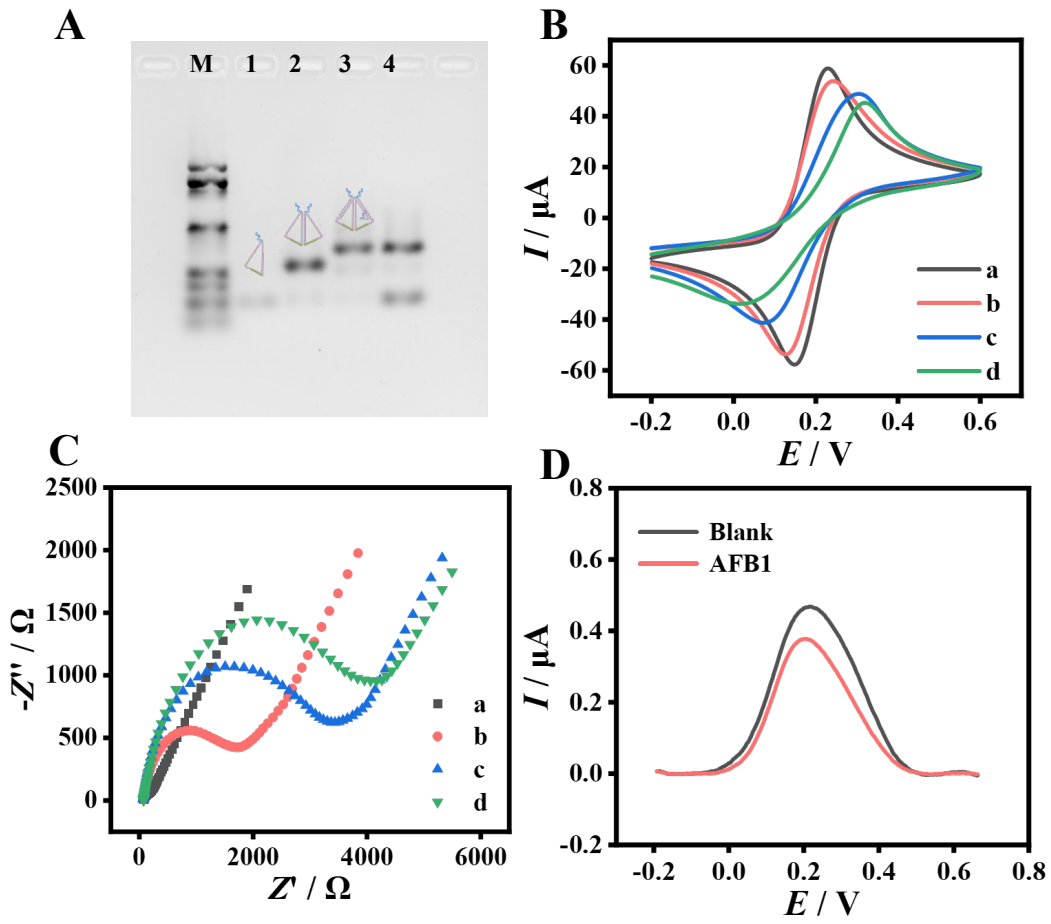


Figure S2. Characterization of 45nt-ATDN. (A) AGE. (B) CV and (C) EIS response of (a) bare Au electrode, (b) 45nt-ATDN+SP/Au, (c) MCH/45nt-ATDN+SP/Au, (d) AFB1/MCH/45nt-ATDN+SP/Au. (D) SWV in the presence and absence of 10 pg mL^{-1} AFB1.

Stepwise Characterization and Feasibility of the polyA.

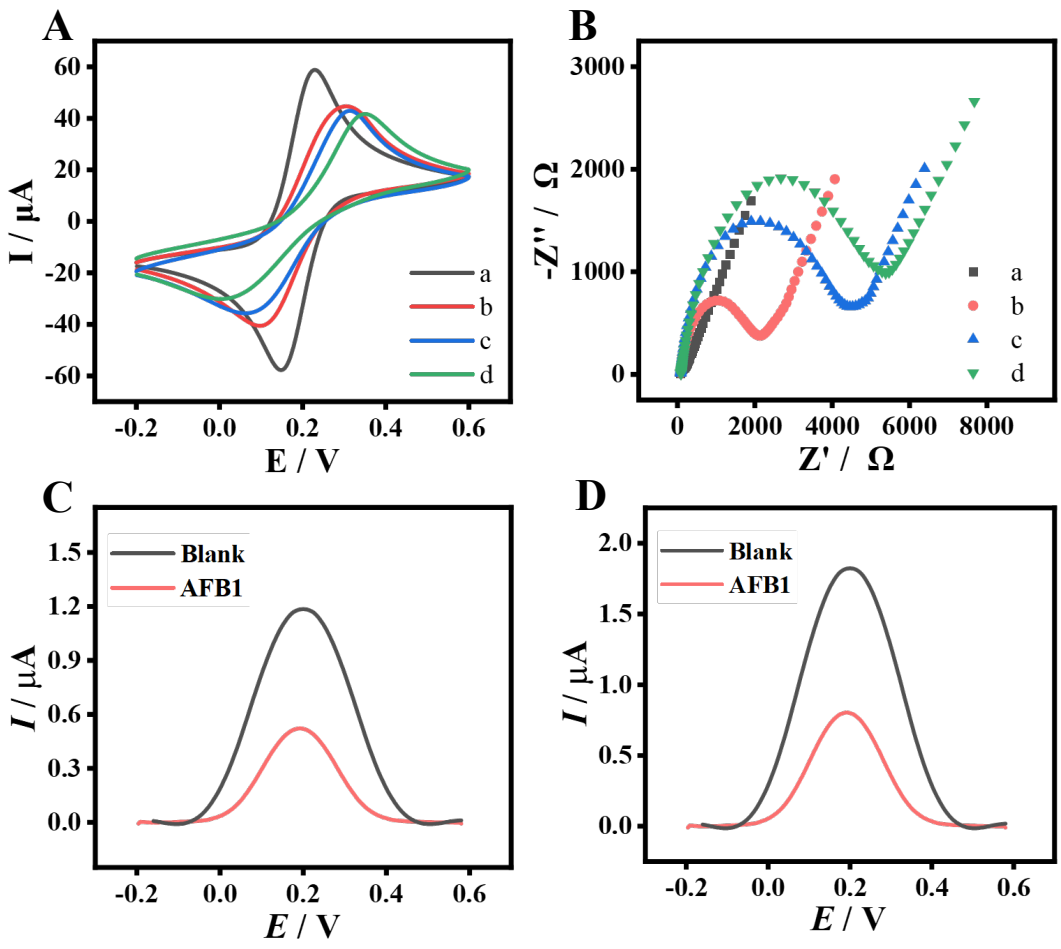


Figure S3. (A) CV and (B) EIS response of polyA: (a) bare Au electrode, (b) polyA+SP/Au, (c) MCH/polyA +SP/Au, (d) AFB1/MCH/polyA +SP/Au. SWV of (C) 1 μM polyA and (D) 2.5 μM polyA in the presence and absence of 10 pg mL^{-1} AFB1.

Stepwise Characterization and Feasibility of TDN.

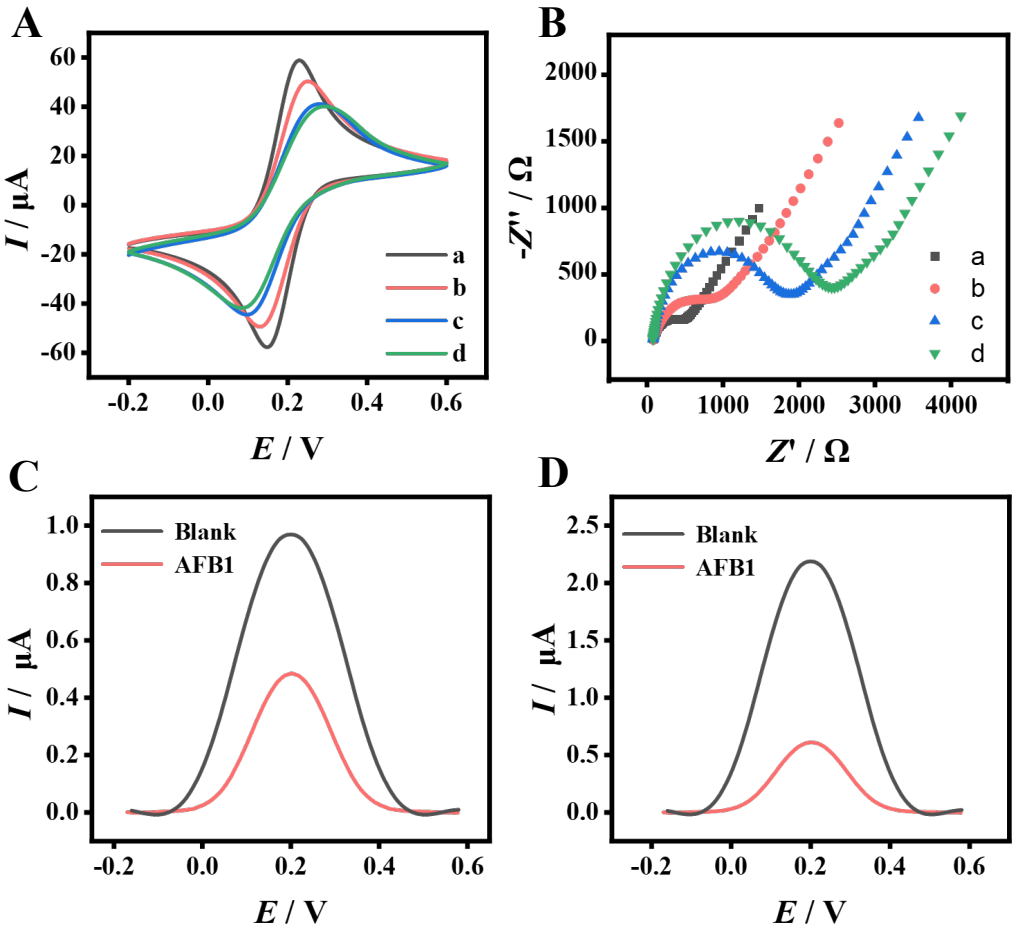


Figure S4. (A) CV and (B) EIS response of TDN: (a) bare Au electrode, (b) TDN+SP/Au, (c) MCH/TDN+SP/Au, (d) AFB1/MCH/TDN+SP/Au. SWV of (C) 1 μM TDN and (D) 5 μM TDN in the presence and absence of 10 pg mL^{-1} AFB1.

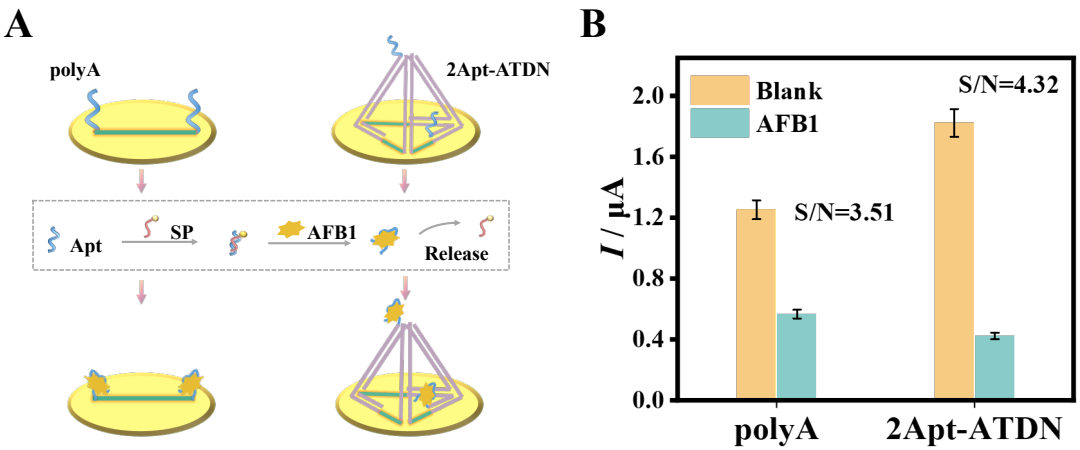


Figure S5. (A) Schematic illustration of the detection process of polyA and ATDN with two aptamers. (B) SWV peak currents of 1 μM polyA and ATDN with two aptamers in the (a) absence and (b) presence of the target AFB1 (10 pg mL^{-1}).

Optimization of the Experimental Conditions.

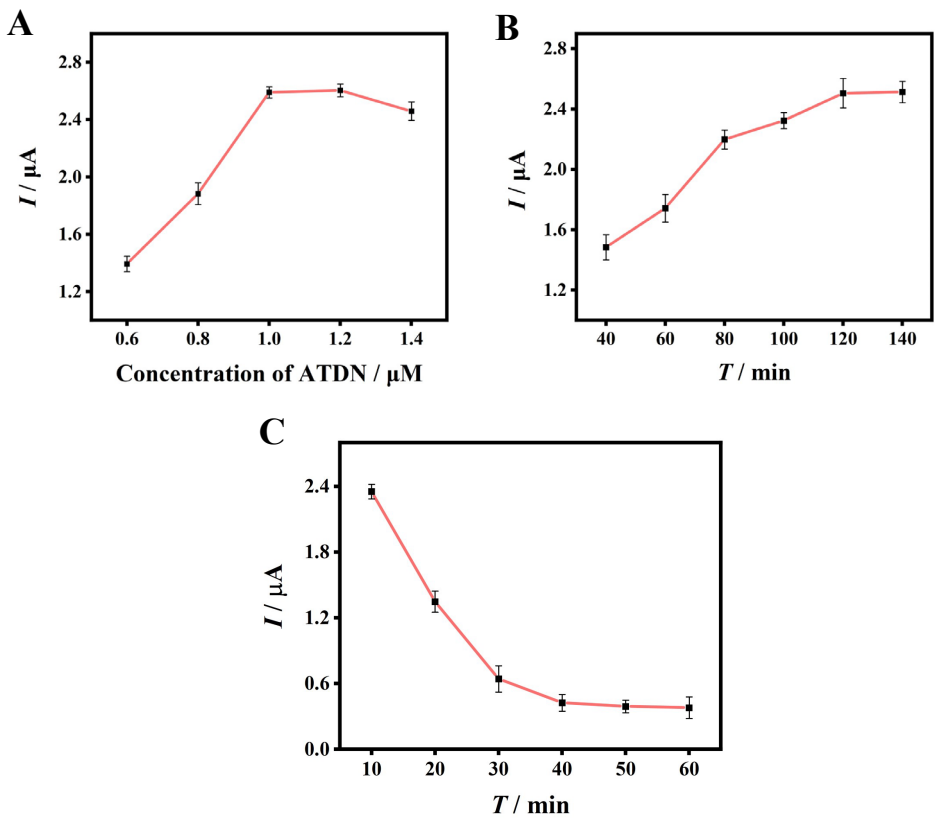
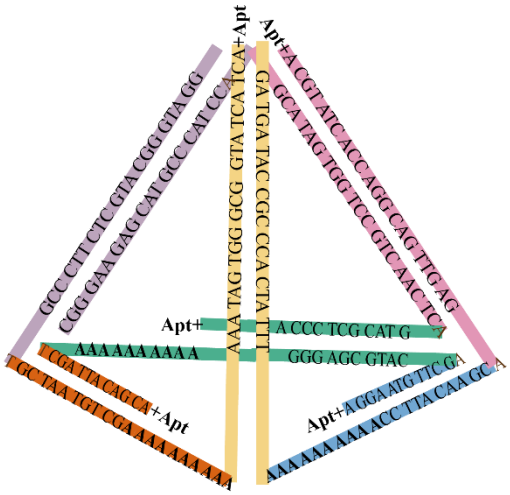


Figure S6. Optimization of experimental conditions: (A) volume of ATDN (1 μM) on the electrochemical response; (B) the reaction time between ATDN and SP; and (C) the detection time of the target (10 pg mL^{-1}AFB1).



113

114 **Fig. S7.** Detailed sequence diagram of tetrahedral DNA nanostructure.

115

Table S1. List of the DNA Sequences

Name	Sequences (5' - 3')
L_{A-30}	CAC GTG TTG TCT CTC TGT GTC TCG TGA GGA ATG TTC GAC ATG CGA GGG AAA AAA AAA ATC GAT TAC AGC ACA CGT GTT GTC TCT CTG TGT CTC GTG
L_{B-30}	CAC GTG TTG TCT CTC TGT GTC TCG TGA CTA CTA TGG CGG GTG ATA AATA AAA AAA AAA GC TGT AAT CGT CGG GAA GAG CAT GCC CAT CC
L_{C-30}	CAC GTG TTG TCT CTC TGT GTC TCG TGA CGT ATC ACC AGG CAG TTG AGA CGA ACA TTC CA AAA AAA AAA TTT TAT CAC CCG CCA TAG TAG
L_{D-30}	5’-CAC GTG TTG TCT CTC TGT GTC TCG TGA CCC TCG CAT GAC TCA ACT GCC TGG TGA TAC GAG GAT GGG CAT GCT CTT CCC G
Aptamer	CAC GTG TTG TCT CTC TGT GTC TCG TG
SP	Fc-GAC ACA GAG AGA CAA
	For the study of ATDN assembly.
L_{A-15}	CAC GTG TTG TCT CTC TGT GTC TCG TGA ACT TAG GAA TGT TCG ACA TGC GAG GGT CCA AAA AAA TCG ATT ACA GCT TGC TAC ACG TGT TGT CTC TCT GTG TCT CGT G
L_{B-15}	CAC GTG TTG TCT CTC TGT GTC TCG TGA CTA CTA TGG CGG GTG ATA AATAAA AAA GCA AGC TGT AAT CGA CGG GAA GAG CAT GCC CAT CC
L_{C-15}	CAC GTG TTG TCT CTC TGT GTC TCG TGA CGT ATC ACC AGG CAG TTG AGA CGA ACA TTC CTA AGT AAA AAT TTT ATC ACC CGC CAT AGT AG
L_{D-15}	CAC GTG TTG TCT CTC TGT GTC TCG TGA TTG GAC CCT CGC ATG ACT CAA CTG CCT GGT GAT ACG AGG ATG GGC ATG CTC TTC CCG

$L_{A\text{-}45}$	CAC GTG TTG TCT CTC TGT GTC TCG TGA GTT CGA CAT GCA AAA AAA AAA AAA AAT CGA TTA CAC GTG TTG TCT CTC TGT GTC TCG TG
$L_{B\text{-}45}$	CAC GTG TTG TCT CTC TGT GTC TCG TGA CTA CTA TGG CGG GTG ATA AAT AAA AAA AAA AAA AAA AAT CGA CGG GAA GAG CAT GCC CAT CC
$L_{C\text{-}45}$	CAC GTG TTG TCT CTC TGT GTC TCG TGA CGT ATC ACC AGG CAG TTG AGA CGA ACA AAA AAA AAA AAA AAT TTT ATC ACC CGC CAT AGT AG
$L_{D\text{-}45}$	CAC GTG TTG TCT CTC TGT GTC TCG TGA GCA TGA CTC AAC TGC CTG GTG ATA CGA GGA TGG GCA TGC TCT TCC CG
SP	Fc-GAC ACA GAG AGA CAA

For the study of signal enhancement

$L_{A\text{-}TDN}$	CAC GTG TTG TCT CTC TGT GTC TCG TGATT CAG ACT TAG GAA TGT TCG ACA TGC GAG GGT CCA ATA CCG ACG ATT ACA GCT TGC TAC ACG
$L_{B\text{-}TDN}$	SH-ACT ACT ATG GCG GGT GAT AAA ACG TGT AGC AAG CTG TAA TCG ACG GGA AGA GCA TGC CCA TCC
$L_{C\text{-}TDN}$	SH-ACG TAT CAC CAG GCA GTT GAG ACG AAC ATT CCT AAG TCT GAA ATT TAT CAC CCG CCA TAG TAG
$L_{D\text{-}TDN}$	SH-ACG GTA TTG GAC CCT CGC ATG ACT CAA CTG CCT GGT GAT ACG AGG ATG GGC ATG CTC TTC CCG
PolyA	CAC GTG TTG TCT CTC TGT GTC TCG TGT AAA AAA AAA AAA AAA AAA AAA AAA AAA AAA TCA CGT GTT GTC TCT CTG TGT CTC GTG
SP	Fc-GAC ACA GAG AGA CAA

Table S2. AFB1 detection in real samples.

Sample	Fortified AFB1 (ng mL^{-1})	Detected by the proposed biosensor (ng mL^{-1})		Detected by HPLC (ng mL^{-1})
		Detected	Recovery	
1	0.5	0.476±0.05	95.2%	0.482
2	1	0.963±0.07	96.3%	0.975
3	5	4.872±0.28	97.4%	4.932
4	10	9.894±0.72	98.9%	9.927

Reference

[1] W.B. Shim, M.J. Kim, H. Mun, M.G. Kim, An aptamer-based dipstick assay for the rapid and simple detection of aflatoxin B1, Biosens Bioelectron, 62(2014) 288-94.

DSPACE

https://dspace.org/

Poly-adenine-mediated tetrahedral DNA nanostructure with multiple target-recognition sites for ultrasensitive and rapid electrochemical detection of Aflatoxin B1

Wang, Kaixuan; Zhu, Nuanfei; Li, Yumo; Zhang, Hu; Wu, Beibei ...

2023-12-01
Elsevier
https://doi.org/10.1016/j.aca.2023.341947
Wang K, Zhu N, Li Y, et al., (2023) Poly-adenine-mediated tetrahedral DNA nanostructure with multiple target-recognition sites for ultrasensitive and rapid electrochemical detection of Aflatoxin B1. Analytica Chimica Acta, Volume 1283, December 2023, Article Number 341947

Downloaded from a DSpace repository. https://dspace.org/